

Rényi Generative Adversarial Networks

Himesh Bhatia^{*}, William Paul^{**}, Fady Alajaji^{*}, Bahman Ghahsifard^{*}, and Philippe Burlina^{**}

^{*}Department of Mathematics and Statistics, Queen’s University, Kingston, ON K7L 3N6, Canada
(himesh.bhatia@queensu.ca, fa@queensu.ca, bahman.ghahsifard@queensu.ca).

^{**}The Johns Hopkins University, Applied Physics Laboratory, Laurel, MD 20723, USA
(william.paul@jhuapl.edu, philippe.burlina@jhuapl.edu)

June 1, 2021

Abstract

We propose a loss function for generative adversarial networks (GANs) using Rényi information measures with parameter α . More specifically, we formulate GAN’s generator loss function in terms of Rényi cross-entropy functionals. We demonstrate that for any α , this generalized loss function preserves the equilibrium point satisfied by the original GAN loss based on the Jensen-Rényi divergence, a natural extension of the Jensen-Shannon divergence. We also prove that the Rényi-centric loss function reduces to the original GAN loss function as $\alpha \rightarrow 1$. We show empirically that the proposed loss function, when implemented on both DCGAN (with L_1 normalization) and StyleGAN architectures, confers performance benefits by virtue of the extra degree of freedom provided by the parameter α . More specifically, we show improvements with regard to: (a) the quality of the generated images as measured via the Fréchet Inception Distance (FID) score (e.g., best FID=8.33 for RényiStyleGAN vs 9.7 for StyleGAN when evaluated over 64×64 CelebA images) and (b) training stability. While it was applied to GANs in this study, the proposed approach is generic and can be used in other applications of information theory to deep learning, e.g., AI bias or privacy.

1 Introduction

Unsupervised learning is the problem of educing information from a large unlabeled dataset and, in the context of generative models, is a relatively new area that has received much attention. Two prominent objectives in generative modeling consist of determining the underlying probability distribution function of a dataset or generating data that mimics it. Classical techniques for the former include maximum likelihood estimators, methods of moments estimators and Bayesian estimators. The main approaches for the latter include generative adversarial networks (GANs) [15], [5], [36], [10], autoencoders/variational autoencoders (VAEs) [22], generative autoregressive models [34], invertible flow based latent vector models [23], or hybrids of the above models [16]. Compared to other approaches, GANs have garnered the most interest (e.g., see surveys in [10], [43], [44]); unlike density estimation models, GANs can efficiently represent distributions confined to a low dimensional manifold [5] and are therefore the focus of this paper.

Prior Work: The original GAN [15] consists of a generative neural network competing with a discriminatory neural network in a min-max game. GANs were enhanced with the introduction of deep convolutional GANs (DCGANs) [36] which use convolutional layers to learn higher dimensional dependencies that are inherent in complex datasets such as images [36]. Although DCGANs produced

better results than other state-of-the-art generative models such as VAEs and autoregressive models, they can be difficult to train and can suffer from mode collapse [5], [44]. Researchers have diligently attempted to fix these problems. For example, StyleGAN [20] changed the architecture of the generative neural network to produce realistic high resolution images, while Wasserstein GAN [5] reduced the problem of mode collapse. Thus the flexibility of GAN’s design allows for innovation and applicability to a wide range of data.

The use of information theory to study and improve neural networks is a relatively new yet promising direction of research; e.g., see [33], [35], [1], [8], [45], [40], [3] and [46] and the references therein. While many GAN loss functions are based on the Jensen-Shannon divergence, there are other divergence measures and tools in information theory that can be directly applied to the design of GANs. The family of loss functions that simplify down to f -divergences were thoroughly studied in [33] and [14]. InfoGAN uses variational mutual information maximization with latency codes to achieve unsupervised representation learning with considerable success [8]. A new least squares loss function that uses the Pearson chi square divergence was examined in [29]. It was shown through experiments that the resulting (LSGAN) network is more stable than DCGAN.

The use of the Rényi divergence in the context of GANs is sparse. Rényi used the simplest set of postulates that characterize Shannon’s entropy and introduced his own entropy and divergence measures (parameterized by its order α) that generalize the Shannon entropy and the KL divergence, respectively [37]. Moreover, the original Jensen-Rényi divergence [18] as well as the identically named divergence [24] used in this paper are non- f -divergence generalizations of the Jensen-Shannon divergence. Traditionally, Rényi’s entropy and divergence have had applications in a wide range of problems, including lossless data compression [7], [9], hypothesis testing [12], [2], error probability [6], and guessing [4], [42]. Recently, the Rényi divergence and its variants (including Sibson’s mutual information) were used to bound the generalization error in learning algorithms [13], and to analyze deep neural networks (DNNs) [45], variational inference [27], Bayesian neural networks [26], and generalized learning vector quantization [31]. However, to the best of our knowledge, there does not exist prior work on generalizing Jensen-Shannon divergence GAN loss functions that are not in the family of f -divergences. This motivates our work.

Contributions: The novel contributions of this paper are described in what follows. We revisit the original GAN generator optimization problem by considering more general parameterized classes of loss functions that subsume the original function as a special case. An important objective is to identify generalized loss functions that can be analytically minimized under an (unconstrained) optimal discriminator, with the minimum theoretically achieved when the generator’s distribution is the true dataset distribution. To this end, we consider a new GAN generator loss function expressed in terms of the negative sum of two Rényi cross-entropy functionals of order α , where $\alpha > 0$ and $\alpha \neq 1$. We show that minimizing this α -parameterized loss function under an optimal discriminator results in the minimization of the Jensen-Rényi divergence [24], which is a natural extension of the Jensen-Shannon divergence as it uses the Rényi divergence instead of the Kullback-Leibler (KL) divergence in its expression. Note that this Jensen-Rényi divergence measure, which reduces to the Jensen-Shannon divergence as α approaches 1, differs from an earlier namesake measure introduced in [18], [17] and defined using the Rényi entropy. We also prove that our generator loss function of order α converges to the original GAN loss function in [15] when $\alpha \rightarrow 1$. Previously, [33] generalized the GAN loss function using the f -divergence measure [11]. However as the Jensen-Rényi divergence is not itself an f -divergence, it can be interpreted as a non- f -divergence generalization of the Jensen-Shannon divergence.

Finally, we implement the newly proposed α -parameterized loss function on DCGAN and StyleGAN [20] architectures, resulting in the so-called *RényiGAN* and *RényiStyleGAN* systems, respectively. Our experiments use the MNIST [25] and CelebA [28] datasets and provide comparisons

with the baseline DCGAN and StyleGAN systems. Experiments show that the Rényi-centric GAN systems perform as well as, or better, than their baseline counterparts in terms of visual quality of the generated images (as measured by the Fréchet Inception Distance, or FID, [19]), particularly when spanning α over a range of values as it helps the avoidance of local minimums. We show that employing L_1 normalization with the Rényi generator loss function confers greater stability, quicker convergence, and better FID scores for both RényiGAN and DCGAN. Consistent stability and slightly improved FID scores are also noted when comparing RényiStyleGAN with StyleGAN. We finally compare these GAN systems with gradient penalty [30], [38], showing that the Rényi-type systems provide substantial reductions in computational training time vis-a-vis the baselines, for similar levels of FID.

2 Notation

Consider a measurable space $(\mathbb{X}, \mathcal{B}(\mathbb{X}), \mu)$, where $\mathcal{B}(\mathbb{X})$ is a σ -algebra on \mathbb{X} and μ is a measure on $(\mathbb{X}, \mathcal{B}(\mathbb{X}))$. For images of size $n \times n$, we will assume $\mathbb{X} \subset \mathbb{R}^n \times \mathbb{R}^n$, $\mathcal{B}(\mathbb{X})$ is the Borel σ -algebra, and μ is the Lebesgue measure. We define the *generative neural network* as a measurable differentiable function $g : (\mathbb{R}^m, \mathcal{B}(\mathbb{R}^m), \mu) \rightarrow (\mathbb{X}, \mathcal{B}(\mathbb{X}), \mu)$ and the *discriminator neural network* as a measurable differentiable $D : (\mathbb{X}, \mathcal{B}(\mathbb{X}), \mu) \rightarrow (\mathcal{A}, \mathcal{B}(\mathcal{A}), \mu)$, where \mathcal{A} is a bounded compact set. Usually, we assume $\mathcal{A} = [0, 1]$. We will use the short form $g : \mathbb{R}^m \rightarrow \mathbb{X}$ and $D : \mathbb{X} \rightarrow \mathcal{A}$ from now on and we assume that all considered probability distributions are absolutely continuous with respect to μ , hence admitting a probability density function.

Let p_z be the *noise probability density* that is the input to the generative neural network, which is usually taken as a multivariate Gaussian distribution of size m . We also denote by p_x the probability density function over the set of images \mathbb{X} , and refer to it as the *true distribution*. Furthermore, we denote by p_g the probability distribution function, which is the distribution of images from the generative neural network, and refer to it as the *generative probability distribution*, or *fake distribution*.

3 Divergence Measures

Divergence measures are used to quantify the dissimilarity between distributions. We recall the definitions of the Rényi divergence and the Rényi (differential) cross-entropy. We also describe the Jensen-Rényi divergence, which is a natural extension of the Jensen-Shannon divergence by virtue of being a mixture of two Rényi divergences. This Jensen-Rényi divergence was recently introduced in [24] for discrete distributions and studied in the context of generalized (Rényi-type) f -divergences. It differs from the identically named divergence studied in [18] and [17], an earlier extension of the Jensen-Shannon divergence consisting of the difference between the Rényi entropy of a mixture of multiple probability distributions and the mixture of the Rényi entropies of the individual distributions. Other recent (but different) extensions of the Jensen-Shannon divergence can be found in [32] and the references therein.

Let p and q be two probability densities with common support $\mathcal{R} \subset \mathbb{R}$ on the Lebesgue measurable space $(\mathbb{R}, \mathcal{B}(\mathbb{R}), \mu)$ and let

$$\text{KL}(p||q) := \int_{\mathcal{R}} p \log \frac{p}{q} d\mu \quad \text{and} \quad h(p; q) := - \int_{\mathcal{R}} p \log q d\mu \quad (1)$$

denote the KL divergence and the differential Shannon cross-entropy between p and q , respectively, where both information measures are assumed to be finite. When $p = q$ almost everywhere (a.e.), then $h(p; q)$ reduces to the differential Shannon entropy of p , denoted by $h(p)$.

Definition 1 The *Rényi divergence of order α* between p and q , where $\alpha > 0$, $\alpha \neq 1$, is given by

$$D_\alpha(p\|q) := \frac{1}{\alpha - 1} \log \left(\int_{\mathcal{R}} p^\alpha q^{1-\alpha} d\mu \right). \quad (2)$$

Note that $D_\alpha(p\|q) \geq 0$ with equality if and only if $p = q$ (a.e.). Furthermore, if $D_\gamma(p\|q) < \infty$ for some $\gamma > 1$, then, as shown in [41], we have that

$$\lim_{\alpha \rightarrow 1} D_\alpha(p\|q) = \text{KL}(p\|q). \quad (3)$$

For simplicity of analysis, we assume in what follows the finiteness of $D_\gamma(\cdot\|\cdot)$ for some $\gamma > 1$ so that convergence of (3) holds. Being a function of an f -divergence, useful properties and bounds on the Rényi divergence can be elucidated from the study of f -divergences, see [39] and related references.

Definition 2 The *differential Rényi cross-entropy of order α* between p and q , where $\alpha > 0$, $\alpha \neq 1$, is given by

$$h_\alpha(p; q) := \frac{1}{1 - \alpha} \log \left(\int_{\mathcal{R}} pq^{\alpha-1} d\mu \right) = \frac{1}{1 - \alpha} \log \left(\mathbb{E}_{A \sim p} (q(A)^{\alpha-1}) \right). \quad (4)$$

Note that $h_\alpha(p; q)$ reduces to the differential Rényi entropy, denoted by $h_\alpha(p)$, when $p = q$ (a.e.). Also, it can be shown that $\lim_{\alpha \downarrow 1} h_\alpha(p; q) = h(p; q)$. The above definition of differential Rényi cross-entropy can be extended (assuming the integral exists) by only requiring q to be a non-negative function (such as a non-normalized density function); in this case we call the resulting measure as the (differential) *Rényi cross-entropy functional* and denote it by $\mathcal{H}_\alpha(p; q)$. Similarly, we henceforth denote the Shannon cross-entropy functional by $\mathcal{H}(p; q)$.

Definition 3 The *Jensen-Rényi divergence of order α* between p and q , where $\alpha > 0$, $\alpha \neq 1$, is given by

$$\text{JR}_\alpha(p\|q) := \frac{1}{2} D_\alpha \left(p \left\| \frac{p+q}{2} \right. \right) + \frac{1}{2} D_\alpha \left(q \left\| \frac{p+q}{2} \right. \right). \quad (5)$$

By the non-negativity of the Rényi divergence, it follows by definition that $\text{JR}_\alpha(p\|q) \geq 0$ with equality if and only if $p = q$ (a.e.). Finally since $\lim_{\alpha \rightarrow 1} D_\alpha(p\|q) = \text{KL}(p\|q)$, we have that

$$\lim_{\alpha \rightarrow 1} \text{JR}_\alpha(p\|q) = \text{JSD}(p\|q), \quad (6)$$

where

$$\text{JSD}(p\|q) := \frac{1}{2} \text{KL} \left(p \left\| \frac{p+q}{2} \right. \right) + \frac{1}{2} \text{KL} \left(q \left\| \frac{p+q}{2} \right. \right) \quad (7)$$

is the Jensen-Shannon divergence.

4 RényiGAN: Theoretical Results

We are now ready to introduce and analyze the RényiGAN system with parameter $\alpha > 0$, $\alpha \neq 1$, which uses (differential) Rényi cross-entropy loss functionals and the Jensen-Rényi divergence measure. Recall that in original GAN, the discriminator aims to classify fake images as 0 and real images as 1 by maximizing the negative sum of two *Shannon cross-entropy functionals*, and the generator tries

to minimize the loss function by making the discriminator label fake generated images as 1. Hence the GAN optimization problem consists of solving the following minimax game:

$$\min_g \max_D V(D, g) \quad (8)$$

where

$$V(D, g) := \mathbb{E}_{A \sim p_x} [\log(D(A))] + \mathbb{E}_{B \sim p_z} [\log(1 - D(g(B)))] \quad (9)$$

$$= -(\mathcal{H}(p_x, D) + \mathcal{H}(p_z, 1 - D \circ g)) \quad (10)$$

and \circ denotes functional composition.

In RényiGAN, we use the same loss function $V(D, g)$ as in GAN for the discriminator. Instead, RényiGAN's generator tries to induce the discriminator to classify the fake images as 1 by minimizing the negative sum of the two Rényi cross-entropy functionals $\mathcal{H}_\alpha(p_x, D)$ and $\mathcal{H}_\alpha(p_z, 1 - D \circ g)$, hence generalizing the original GAN loss function in (10) by employing a richer α -parameterized class of information functionals.

Using the above Rényi-centric loss function allows us to control the shape of the generator's loss function via the α parameter. If the discriminator converges to the optimal discriminator, we show analytically that for any $\alpha > 0$, $\alpha \neq 1$, the optimal generator induces a probability distribution that perfectly mimics the true dataset distribution, as in GAN. This result is formalized as follows.

Theorem 1 *Let $\alpha > 0$, $\alpha \neq 1$. Consider the following optimization problems for training the neural networks $g : \mathbb{R}^m \rightarrow \mathbb{X}$ and $D : \mathbb{X} \rightarrow (0, 1)$:*

$$\max_D V(D, g) = \max_D \left(\mathbb{E}_{A \sim p_x} [\log(D(A))] + \mathbb{E}_{B \sim p_z} [\log(1 - D(g(B)))] \right) \quad (11)$$

$$\min_g V_\alpha(D, g) := \min_g -(\mathcal{H}_\alpha(p_x, D) + \mathcal{H}_\alpha(p_z, 1 - D \circ g)) \quad (12)$$

$$= \min_g \left(\frac{1}{\alpha - 1} \log \left[\mathbb{E}_{A \sim p_x} (D(A)^{\alpha-1}) \right] + \frac{1}{\alpha - 1} \log \left[\mathbb{E}_{B \sim p_z} ((1 - D(g(B)))^{\alpha-1}) \right] \right). \quad (13)$$

Then (11) is maximized by $D^* = p_x / (p_x + p_g)$, where p_g is the generator's distribution. Furthermore, if $D = D^*$, then (13) simplifies to $\min_{p_g} 2\text{JR}_\alpha(p_x \| p_g) - 2\log(2)$ which is achieved by $p_g^* = p_x$.

Proof of Theorem 1 is provided in the Appendix

Interpretation: This theorem implies that the introduction of the new loss function does not alter the underlying global equilibrium point of RényiGAN when compared to the classical GAN (which uses a Shannon-centric loss function), namely that the minimum is theoretically achieved when the generator's distribution is the true dataset distribution.

We next show that the above Rényi-type loss function $V_\alpha(D, g)$ in (13) recovers the original GAN loss function $V(D, g)$ when the parameter $\alpha \rightarrow 1$.

Theorem 2 *Assuming $V(D, g) < \infty$, then*

$$\lim_{\alpha \downarrow 1} V_\alpha(D, g) = V(D, g). \quad (14)$$

Moreover, if $\mathbb{E}_{A \sim p_x} \left(\frac{1}{D(A)} \right) < \infty$ and $\mathbb{E}_{B \sim p_z} \left(\frac{1}{1 - D(g(B))} \right) < \infty$ then

$$\lim_{\alpha \uparrow 1} V_\alpha(D, g) = V(D, g). \quad (15)$$

Proof of Theorem 2 is provided in the Appendix

5 Methods

We used the MNIST [25] and CelebA [28] datasets to investigate our new loss functions. We kept the structure of the generator and discriminator neural networks constant when testing on each dataset. For MNIST, we implemented DCGAN with and without gradient penalty [38], [30] (denoted by DCGAN-GP) for comparison. Also, for CelebA, we implemented StyleGAN [20] with and without gradient penalty (denoted by StyleGAN-GP) for comparison.

For MNIST, in addition to using RényiGAN with a fixed value of α , we implemented RényiGAN while altering α for every epoch of the simulation. This changes the shape of the loss function of the generator. However, changing α does not affect the global minimum as for all $\alpha > 0$, the global minimum is realized when $p_x = p_g$. Note that the algorithm skips the case $\alpha = 1.0$, which corresponds to the DCGAN loss function. Assuming that a generator $p_g \neq p_x$ is realized such that it is not a local minimum of $V_\alpha(D, g)$ for all $\alpha > 0$, then changing α every epoch creates non-zero gradients at previous local minimums, hence helping the algorithm overcome the problem of getting stuck in local minimums. We denote such implemented system by RényiGAN- $[\beta_1, \beta_2]$, with the α value starting at $\alpha = \beta_1$ and ranging over the interval $[\beta_1, \beta_2]$. Also RényiGAN- α denotes a system using a single value of α for all epochs.

One goal was to examine whether the new generalized loss functions have appreciable benefits over the classical GAN loss function and whether it provides better training stability. It is known that DCGAN exhibits stability issues which motivate us to investigate modifications to the loss functions involving the addition of the L_1 norm. Specifically, those stability issues arise when the GAN generator tries to minimize its cost function to $-\infty$ by labelling $D(g(z)) = 1$ for all fake images $g(z)$. In the early stages of the simulations, if the discriminator does not successfully converge to its optimal value and the generator is able to induce the discriminator to label poorly generated images as 1, then in later epochs, once the discriminator converges to its optimal value and is able to tell apart real and fake images perfectly, the generator’s loss function produces no gradients. In other words, the optimal discriminator does not allow the generator to improve the quality of fake images which leads to the discriminator winning problem. A similar argument was noted in [5]. Thus to remedy the stability problem, we modified the Rényi loss function $V_\alpha(D, g)$ in (12) by taking the L_1 norm of its deviation from $-2 \log(2)$, its theoretically minimal value predicted by Theorem 1; this yields the following minimization problem for the generator network:

$$\min_g \left| V_\alpha(D, g) - (-2 \log 2) \right| = \min_g \left| (-\mathcal{H}_\alpha(p_x, D) + \log 2) + (-\mathcal{H}_\alpha(p_z, 1 - D \circ g) + \log 2) \right|. \quad (16)$$

Using the L_1 norm ensures that the generator’s loss function does not try to label its images as 1, but rather tries to label them as 1/2. Hence in the early training stages, if the generator converges to images that are labelled 1/2 by the discriminator, then in the later stages, if the discriminator converges to its theoretical optimal value (given in Theorem 1), the generator’s loss function has non-zero gradient updates and is only able to label fake images as 1/2 when $p_g = p_x$. We denote the resulting scheme under (16) by RényiGAN- L_1 .

In summary, we considered three group evaluations with six different loss functions within each group. Group 1 has RényiGAN-0.5- L_1 , RényiGAN-3.0- L_1 , RényiGAN-[0, 0.9]- L_1 , RényiGAN-[0, 3.0]- L_1 , RényiGAN-[1.1, 4]- L_1 , and DCGAN- L_1 . Group 2 has the six original loss functions with gradient penalty and Group 3 has gradient penalty and L_1 normalization incorporated in the loss functions. The equations of these loss functions can be found in the Appendix along with the training procedure. The RényiGAN- α and RényiGAN- $[\beta_1, \beta_2]$ training procedures without/with generator L_1 normalization and discriminator gradient penalty are shown in Algorithms 1 and 2, respectively. Tables 3 and 4 in the Appendix detail the generator’s and discriminator’s architecture used for testing our loss functions on MNIST.

Finally, information about experiments on CelebA, such as the description of the baseline StyleGAN computing architecture we used, can be found in Tables 5, 6 and 7 in the Appendix.

6 Experiments

6.1 MNIST

We used FID scores to objectively evaluate the quality of the generated images and to compare the rate at which the new networks converge to their optimal scores. As MNIST consists of $28 \times 28 \times 1$ images, we did not pre-process the data by passing the images through an Inception network as the Inception network is trained on realistic looking images, such as animals or human faces, rather than handwritten images. Instead we used the raw real and generated images to calculate the FID scores. We ran 10 experiments (trials) and control the random seeds for each trial. For each trial and each epoch, we calculated the FID scores.

Considering first the DCGAN baseline, we observed that for MNIST, DCGAN exhibits unstable training as was expected and that the addition of the Rényi loss is able to ameliorate convergence but has similar instabilities. More specifically, RényiGAN-[0, 3] converged in three out of ten trials, achieving an average best FID scores of 1.36, while DCGAN experienced mode collapse in all ten trials.

We then compared the use of the Rényi loss function in conjunction with the aforementioned algorithms. For a single trial, we considered the lowest FID score over 250 epochs, which we call the best FID score for that trial. We took the average and variance of all 10 best FID scores, and the median and variance of the epoch when the best FID score is achieved and present the results in Table 1. Additional results, such as the FID score statistics for all trials (Table 8), representative samples of generated images (Figure 3) and the graphs of FID score versus epoch (Figure 2), are included in the Appendix. We remark that from Table 1, that in all cases the use of the Rényi loss function improves the FID performance and training convergence characteristics.

6.2 CelebA

We ran each variant of StyleGAN for three trials, using the same seeds in each case for better comparison of results.

Similar to the experiment on MNIST, we took the best FID for each trial and include them along with the median best FID in Table 2. Sample generated images by RényiStyleGAN and StyleGAN are presented in Figure 4 in the Appendix. We note that, as for the case of MNIST, for all baselines in Table 2, the use of the Rényi loss function enhances FID performance and significantly improves the convergence dynamics as seen in Figure 1.

7 Discussion

Applying the L_1 normalization drastically improved the convergence of all networks with no computational overhead. In fact, on average over 250 epochs and 10 trials, adding L_1 normalization decreased the computing time for one epoch by 9.52%. Using L_1 normalization also has the added benefit of networks converging to an optimal FID value in fewer epochs than any other convergent networks across all groups. We note that RényiGAN-[0, 3]- L_1 outperforms all other loss functions in its group and it is sufficient to train it within 50 epochs. The development of a rigorous mathematical theory that describes this phenomenon is an interesting future direction to better understand the dynamics of GANs. In Group 2, RényiGAN-GP-[1.1, 4] performs among the best compared to other

Table 1: RényiGAN experiments on MNIST: the average and variance of the best FID scores and the median and variance of the epoch this occurs taken over 10 trials.

	Average best FID score	Best FID scores variance	Median epoch	Epoch variance
RényiGAN-0.5- L_1	2.21	7.57×10^{-3}	31.50	160.04
RényiGAN-3.0- L_1	1.80	2.95 $\times 10^{-3}$	48.00	4611.16
RényiGAN-[0, 0.9]- L_1	2.16	6.36×10^{-3}	31.50	242.89
RényiGAN-[0, 3]-L_1	1.77	4.90×10^{-3}	34.00	36.80
RényiGAN-[1.1, 4]- L_1	1.81	3.18×10^{-3}	147.50	7326.96
DCGAN- L_1	1.93	3.83×10^{-3}	34.50	2605.61
RényiGAN-GP-0.5	1.37	4.36×10^{-3}	217.00	606.64
RényiGAN-GP-3.0	1.36	2.51×10^{-3}	219.00	751.09
RényiGAN-GP-[0, 0.9]	1.36	2.74×10^{-3}	233.00	423.96
RényiGAN-GP-[0, 3]	1.41	3.09×10^{-3}	204.00	1209.69
RényiGAN-GP-[1.1, 4]	1.36	4.35×10^{-3}	200.00	1144.81
DCGAN-GP	1.36	1.45 $\times 10^{-3}$	228.00	342.56
RényiGAN-GP-0.5- L_1	1.18	2.95×10^{-3}	211.50	624.45
RényiGAN-GP-3.0-L_1	1.17	3.62×10^{-3}	231.00	609.61
RényiGAN-GP-[0, 0.9]- L_1	1.19	3.61×10^{-3}	226.50	1425.36
RényiGAN-GP-[0, 3]- L_1	1.22	6.33×10^{-3}	237.00	1075.09
RényiGAN-GP-[1.1, 4]- L_1	1.20	3.46×10^{-3}	213.50	1326.36
DCGAN-GP- L_1	1.18	1.58 $\times 10^{-3}$	217.00	1263.05

RényiGAN-GP variants, with an identical performance to DCGAN-GP. Moreover, on average it converges to its best FID score in fewer epochs than DCGAN-GP. Note, however, that the use of gradient penalty increases the computation time by 17% compared to the previous group. The best performing network in terms of FID score is RényiGAN-GP-3.0- L_1 , seen in the Group 3 results of Table 1. Note that RényiGAN-GP-0.5- L_1 , RényiGAN-GP-3.0- L_1 , RényiGAN-GP-[0, 0.9]- L_1 , and DCGAN-GP- L_1 exhibit quite similar FID scores as the difference of 0.02 FID score has no qualitative effect on the generated images. However, on average, DCGAN-GP- L_1 converges to its optimal FID score in fewer epochs than its counterparts in its group.

In summary, the extra degree of freedom provided by the α parameter yields a variety of new loss functions and algorithmic designs that gives equivalent or better FID scores in fewer epochs. Note that a difference of 0.20 FID score has no noticeable qualitative difference in MNIST generated images. In the first group, DCGAN- L_1 and RényiGAN-[0, 3]- L_1 's generated images are qualitatively similar. Correspondingly, there is no discernible difference between Groups 2 and 3. The perceivable disparity in quality is between the first and the second group, which has a difference in FID score of 0.41; see Figure 3 in the Appendix. Moreover, the meaning of FID scores diminishes after a certain threshold when the generated images are realistic. It is useful to conduct experiments to determine these thresholds for commonly used datasets. Hence, the greatest advantage of RényiGAN when

Table 2: RényiStyleGAN experiments on the CelebA: best FID over each run seen over three trials. We do not run as many trials as the previous RényiGAN experiments due to the significantly increased computation time. RényiStyleGAN- x denotes the run using our proposed loss with $\alpha = x$, and GP denotes using gradient penalty and the minibatch deviation layer.

Best FID Over Run	Trial 1	Trial 2	Trial 3	Median FID
RényiStyleGAN-3.0	9.67	9.60	10.14	9.67
RényiStyleGAN-9.0	11.22	8.33	11.59	11.22
StyleGAN	16.20	9.70	17.90	16.20
RényiStyleGAN-3.0-GP	3.91	3.92	3.82	3.91
StyleGAN-GP	4.06	3.90	3.85	3.90

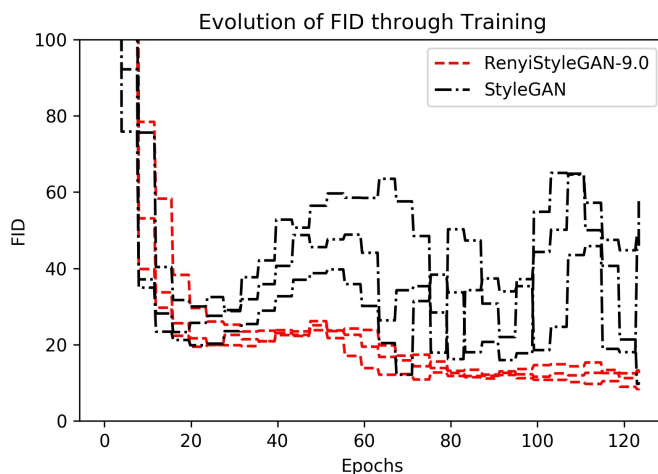


Figure 1: Evolution of FID through training for multiple trials of RényiStyleGAN-9.0 and StyleGAN.

applied to MNIST is its ability to consistently converge to realistic and diverse generated images quicker than DCGAN.

For CelebA, we observe that RényiStyleGAN (with $\alpha > 1$) outperforms StyleGAN in terms of FID scores, with setting $\alpha = 3.0$ achieving the best median FID. Note that when $\alpha < 1$, there are some choices of α that yield a sub-par performance (e.g., see a sample generated image for $\alpha = 0.5$ in Figure 4a in the Appendix). Further investigation on the best range of values of α for the StyleGAN architecture is necessary.

Figure 1 shows that RényiStyleGAN performs consistently and does not display the erratic unstable behaviour of regular StyleGAN. One explanation for the difference in performance dynamics is that the Rényi loss dampens the loss of each individual sample in the batch, reducing the effect of samples that may be given spurious gradient directions. Combined with our use of the Adam optimizer to keep track of the gradient variance, the overall effect that dampening has on the entire objective function is normalized out, while still maintaining the benefit of dampening individual samples from the generator. Additionally, as we close the gap between StyleGAN with and without gradient penalty, one benefit of not needing gradient penalty is the significant reduction in computation time: RényiStyleGAN-3.0 takes roughly 25.63 hours without gradient penalty and 31.8 hours with gradient penalty, yielding a 24% increase in computation time when using gradient

penalty. Lastly, both RényiStyleGAN-GP and StyleGAN-GP perform identically; see also Figure 4 in the Appendix.

8 Conclusion

In this paper, a GAN generator loss function based on Rényi cross-entropy measures of order α ($\alpha > 0$ and $\alpha \neq 1$) was proposed, analyzed and implemented. It was shown that the classical GAN analytical minimax result expressed in terms of minimizing the Jensen-Shannon divergence between the generator and the unconstrained discriminator distributions can be generalized for any α in terms of the broader Jensen-Rényi divergence, with the original GAN loss function provably recovered in the limit of α approaching 1. We demonstrated via experiments on MNIST and CelebA datasets that the proposed loss function yields performance improvements over the original GAN loss function in terms of the quality of the generated images and training stability. In particular, RényiGAN used with L_1 normalization does not need gradient penalty to reduce the GAN mode collapse problem. Furthermore, RényiStyleGAN provides more robust convergence dynamics than StyleGAN and can dispose of using gradient penalty without affecting image fidelity while requiring considerably less training time. Finally, we note that the Rényi-centric approach studied in this work can be judiciously adopted to other deep learning neural network architectures.

References

- [1] Alessandro Achille and Stefano Soatto. Where is the information in a deep neural network? *arXiv e-prints*, page arXiv preprint arXiv:1905.12213, May 2019.
- [2] Fady Alajaji, Po-Ning Chen, and Ziad Rached. Csiszár’s cutoff rates for the general hypothesis testing problem. *IEEE Transactions on Information Theory*, 50(4):663–678, 2004.
- [3] Alexander A. Alemi, Ian Fischer, Joshua V Dillon, and Kevin Murphy. Deep variational information bottleneck. In *International Conference on Learning Representations*, 2017.
- [4] Erdal Arıkan. An inequality on guessing and its applications to sequential decoding. *IEEE Transactions on Information Theory*, 42(1):99–105, 1996.
- [5] Martin Arjovsky, Soumith Chintala, and Léon Bottou. Wasserstein generative adversarial networks. In *Proceedings of the 34th International Conference on Machine Learning*, volume 70, pages 214–223, Aug. 2017.
- [6] M. Ben-Bassat and J. Raviv. Rényi’s entropy and the probability of error. *IEEE Transactions on Information Theory*, 24(3):324–331, Sep 2006.
- [7] Lorne L. Campbell. A coding theorem and Rényi’s entropy. *Information and Control*, 9:423–429, 1965.
- [8] Xi Chen, Yan Duan, Rein Houthoofd, John Schulman, Ilya Sutskever, and Pieter Abbeel. InfoGAN: Interpretable representation learning by information maximizing generative adversarial nets. In *Advances in Neural Information Processing Systems*, pages 2172–2180, 2016.
- [9] Thomas A. Courtade and Sergio Verdú. Cumulant generating function of codeword lengths in optimal lossless compression. *Proc. IEEE International Symposium on Information Theory*, pages 2494–2498, July 2014.

- [10] Antonia Creswell, Tom White, Vincent Dumoulin, Kai Arulkumaran, Biswa Sengupta, and Anil A Bharath. Generative adversarial networks: An overview. *IEEE Signal Processing Magazine*, 35(1):53–65, 2018.
- [11] Imre Csiszár. Information-type measures of difference of probability distributions and indirect observations. *Studia Sci. Math. Hungarica*, 2:299–318, Jan. 1967.
- [12] Imre Csiszár. Generalized cutoff rates and Rényi’s information measures. *IEEE Transactions on Information Theory*, 41(1):26–34, 1995.
- [13] Amedeo Roberto Esposito, Michael Gastpar, and Ibrahim Issa. Robust generalization via α -mutual information. In *Proceedings of the International Zurich Seminar on Information and Communication*, pages 96–100, February 2020.
- [14] Farzan Farnia and David Tse. A convex duality framework for GANs. In *Advances in Neural Information Processing Systems 31*, pages 5248–5258, 2018.
- [15] Ian Goodfellow, Jean Pouget-Abadie, Mehdi Mirza, Bing Xu, David Warde-Farley, Sherjil Ozair, Aaron Courville, and Yoshua Bengio. Generative adversarial nets. In *Advances in Neural Information Processing Systems*, volume 27, pages 2672–2680, 2014.
- [16] Aditya Grover, Manik Dhar, and Stefano Ermon. Flow-GAN: Combining maximum likelihood and adversarial learning in generative models. In *Thirty-Second AAAI Conference on Artificial Intelligence*, 2018.
- [17] A. Ben Hamza and Hamid Krim. Jensen-Rényi divergence measure: Theoretical and computational perspectives. In *Proceedings of the IEEE International Symposium on Information Theory*, July 2003.
- [18] Yun He, A. Ben Hamza, and Hamid Krim. A generalized divergence measure for robust image registration. *IEEE Transactions on Signal Processing*, pages 1211 – 1220, 2003.
- [19] Martin Heusel, Hubert Ramsauer, Thomas Unterthiner, Bernhard Nessler, and Sepp Hochreiter. GANs trained by a two time-scale update rule converge to a local nash equilibrium. In *Advances in Neural Information Processing Systems*, pages 6626–6637, 2017.
- [20] Tero Karras, Samuli Laine, and Timo Aila. A style-based generator architecture for generative adversarial networks. In *The IEEE Conference on Computer Vision and Pattern Recognition (CVPR)*, June 2019.
- [21] Diederik P. Kingma and Jimmy Ba. Adam: A method for stochastic optimization. In *Proceedings of the 3rd International Conference on Learning Representations (ICLR)*, arXiv preprint arXiv:1412.6980, 2015.
- [22] Diederik P. Kingma and Max Welling. Auto-encoding variational bayes. In *Proceedings of the 2nd International Conference on Learning Representations (ICLR)*, 2014.
- [23] Durk P Kingma and Prafulla Dhariwal. Glow: Generative flow with invertible 1x1 convolutions. In *Advances in Neural Information Processing Systems*, pages 10215–10224, 2018.
- [24] Pawel A. Kluza. On Jensen-Rényi and Jeffreys-Rényi type f -divergences induced by convex functions. *Physica A: Statistical Mechanics and its Applications*, 2019.

- [25] Yann LeCun and Corinna Cortes. MNIST handwritten digit database, 1998.
- [26] Yingzhen Li and Yarín Gal. Dropout inference in Bayesian neural networks with alpha-divergences. In *Proceedings of the 34th International Conference on Machine Learning*, volume 70, pages 2052–2061, International Convention Centre, Sydney, Australia, Aug. 2017. PMLR.
- [27] Yingzhen Li and Richard E. Turner. Rényi divergence variational inference. In *Advances in Neural Information Processing Systems*, volume 29, pages 1073–1081, 2016.
- [28] Ziwei Liu, Ping Luo, Xiaogang Wang, and Xiaoou Tang. Deep learning face attributes in the wild. In *Proceedings of International Conference on Computer Vision (ICCV)*, December 2015.
- [29] Xudong Mao, Qing Li, Haoran Xie, Raymond Y.K. Lau, Zhen Wang, and Stephen Paul Smolley. Least squares generative adversarial networks. In *The IEEE International Conference on Computer Vision (ICCV)*, Oct 2017.
- [30] Lars Mescheder, Andreas Geiger, and Sebastian Nowozin. Which training methods for gans do actually converge? In *Proceedings of the 35th International Conference on Machine Learning*, 2018.
- [31] E. Mwebaze, P. Schneider, F. M. Schleif, S. Haase, T. Villmann, and M. Biehl. Divergence based learning vector quantization. In *18th European Symposium on Artificial Neural Networks (ESANN 2010)*, pages 247–252, 2010.
- [32] Frank Nielsen. On a generalization of the Jensen-Shannon divergence. *arXiv preprint arXiv:1912.00610*, Dec. 2019.
- [33] Sebastian Nowozin, Botond Cseke, and Ryota Tomioka. f -GAN: Training generative neural samplers using variational divergence minimization. In *Advances in Neural Information Processing Systems*, volume 29, pages 271–279. Curran Associates, Inc., 2016.
- [34] Aaron van den Oord, Sander Dieleman, Heiga Zen, Karen Simonyan, Oriol Vinyals, Alex Graves, Nal Kalchbrenner, Andrew Senior, and Koray Kavukcuoglu. Wavenet: A generative model for raw audio. *arXiv preprint arXiv:1609.03499*, 2016.
- [35] Jose C. Principe. *Information Theoretic Learning: Rényi’s Entropy and Kernel Perspectives*. Springer Science and Business Media, 2010.
- [36] Alec Radford, Luke Metz, and Soumith Chintala. Unsupervised representation learning with deep convolutional generative adversarial networks. In *International Conference on Image and Graphics (ICIG)*, pages 97–108, 2017.
- [37] Alfréd Rényi. On measures of entropy and information. In *Proceedings of the Fourth Berkeley Symposium on Mathematical Statistics and Probability*, volume 1, pages 547–561, 1961.
- [38] Kevin Roth, Aurelien Lucchi, Sebastian Nowozin, and Thomas Hofmann. Stabilizing training of generative adversarial networks through regularization. *31st Conference on Neural Information Processing Systems*, November 2017.
- [39] Igal Sason. On f -divergences: Integral representations, local behavior, and inequalities. *Entropy*, 20, May 2018.
- [40] Naftali Tishby and Noga Zaslavsky. Deep learning and the information bottleneck principle. In *Proceedings of the 2015 IEEE Information Theory Workshop*, April 2015.

- [41] Tim van Erwen and Peter Harremos. Rényi divergence and Kullback-Leibler divergence. *IEEE Transactions on Information Theory*, 60(7):3797 – 3820, June 2014.
- [42] Sergio Verdú. α -mutual information. In *Proceedings of the IEEE Information Theory and Applications Workshop (ITA)*, February 2015.
- [43] Zhengwei Wang, Qi She, and Tomas E. Ward. Generative adversarial networks in computer vision: A survey and taxonomy. *arXiv preprint arXiv:1906.01529v3*, 2020.
- [44] Maciej Wiatrak, Stefano V. Albrecht, and Andrew Nystrom. Stabilizing generative adversarial network training: A survey. *arXiv preprint arXiv:1910.00927v2*, 2020.
- [45] Kristoffer Wickstrom, Sigurd Lokse, Michael Kampffmeyer, Shujian Yu, Jose Principe, and Robert Jensen. Information plane analysis of deep neural networks via matrix-based Rényi’s entropy and tensor kernels. *arXiv preprint arXiv:1909.11396*, Sep. 2019.
- [46] Abdellatif Zaidi, Iñaki Estella-Aguerri, and Shlomo Shamai (Shitz). On the information bottleneck problems: Models, connections, applications and information theoretic views. *Entropy*, 22, January 2020.

9 Appendix

9.1 Experimental setup

For the MNIST dataset, we used seed 123, 5005, 1600, 199621, 60677, 20435, 15859, 33764, 79878, 36123 for trials 1 to 10, respectively. We used NVIDIA GP100 GPUs and Intel Xeon 2.6 GHz E7 – 8867 v3 CPUs.

For the MNIST dataset, we used the original $28 \times 28 \times 1$ image size and created our own architectures for the generator and discriminator networks. We initialized the weights of each layer by using a Gaussian random variable with mean 0 and standard deviation 0.01. We also used the Adam optimizer [21] with a learning rate of 2×10^{-4} , $\beta_1 = 0.5$, $\beta_2 = 0.999$, and $\epsilon = 1 \times 10^{-7}$ for both networks. The batch size was chosen to be 100 for the 60,000 MNIST images. The total number of epochs was 250 for the MNIST images.

For CelebA, we used seeds 1000, 2000, and 3000 for trials 1, 2, and 3 respectively. We used NVIDIA V100 GPUs. As mentioned in the main text, we took the publicly available code from <https://github.com/NVlabs/stylegan> and modified to introduce the Rényi loss. Consequently, the architectural defaults were left in place. We used 4 gpus to train each trial, with a total batch size of 128. We did not use progressive growing, but instead a fixed resolution of 64×64 . We used Adam with a learning rate of 0.001, $\beta_1 = 0.0$, $\beta_2 = 0.99$ and $\epsilon = 10^{-8}$. We do not mirror the images during training, and train for a total of 25 million images or roughly 120 epochs.

9.2 Neural network architectures implemented on MNIST dataset

We shorten some of the common terms used to describe the layers of the networks. A fully connected layer in a neural network is denoted by FC, while we have used upconv. to denote a deconvolution layer; finally, LeakyReLU denotes the activation function $f : \mathbb{R} \rightarrow \mathbb{R}$ defined as

$$f(x) = \begin{cases} 0.3x & \text{if } x < 0, \\ x & \text{if } x \geq 0, \end{cases}$$

and ReLU denotes the activation function $g : \mathbb{R} \rightarrow \mathbb{R}$ defined as

$$g(x) = \begin{cases} 0 & \text{if } x < 0, \\ x & \text{if } x \geq 0. \end{cases}$$

Table 3: The generator’s architecture for MNIST dataset.

GENERATOR
INPUT $7 \times 7 \times 256$ GAUSSIAN NOISE.
RESHAPE INTO $7 \times 7 \times 256$ IMAGE.
5×5 UPCONV. 128 LEAKYRELU, BATCHNORM.
5×5 UPCONV. 64 LEAKYRELU, STRIDE 2, BATCHNORM.
5×5 UPCONV. 1 CHANNEL, <i>tanh</i> ACTIVATION.

Table 4: The discriminator’s architecture for MNIST dataset.

DISCRIMINATOR

INPUT $28 \times 28 \times 1$ GREY IMAGE.
 5×5 CONV. 64 LEAKYRELU, STRIDE 2, BATCHNORM,
DROPOUT 0.3.
 5×5 CONV. 128 LEAKYRELU, STRIDE 2, BATCHNORM,
DROPOUT 0.3.
FC TO ONE OUTPUT, *sigmoid* ACTIVATION.

9.3 Neural network architectures implemented on CelebA dataset

As we took the StyleGAN repository directly and did not change the architectural parameters, we include the details of the default StyleGAN architecture below.

Table 5: G’s mapping network architecture for CelebA dataset.

GENERATOR MAPPING

INPUT 512 GAUSSIAN NOISE L2 NORMALIZED.
512 TO 512 FULLY CONNECTED LAYER LEAKYRELU $\times 8$.

Table 6: G’s synthesis network architecture for CelebA dataset.

GENERATOR SYNTHESIS

CONSTANT TENSOR OF $512 \times 4 \times 4$
 3×3 CONV. 512 LEAKYRELU, STRIDE 1
 3×3 CONV. 512 LEAKYRELU, STRIDE 1
UPSCALE
 3×3 CONV. 512 LEAKYRELU, STRIDE 1
 3×3 CONV. 512 LEAKYRELU, STRIDE 1
UPSCALE
 3×3 CONV. 512 LEAKYRELU, STRIDE 1
 3×3 CONV. 512 LEAKYRELU, STRIDE 1
UPSCALE
 3×3 CONV. 512 LEAKYRELU, STRIDE 1
 3×3 CONV. 512 LEAKYRELU, STRIDE 1
UPSCALE
 3×3 CONV. 512 LEAKYRELU, STRIDE 1
 3×3 CONV. 512 LEAKYRELU, STRIDE 1
 1×1 CONV. 3 LINEAR, STRIDE 1

Table 7: The discriminator’s architecture for CelebA dataset.

DISCRIMINATOR

INPUT $64 \times 64 \times 3$ COLOR IMAGE.
 1×1 CONV. 256 LEAKYRELU, STRIDE 1
 3×3 CONV. 256 LEAKYRELU, STRIDE 1
 3×3 CONV. 512 LEAKYRELU, STRIDE 1
DOWNSCALE
 3×3 CONV. 512 LEAKYRELU, STRIDE 1
 3×3 CONV. 512 LEAKYRELU, STRIDE 1
DOWNSCALE
 3×3 CONV. 512 LEAKYRELU, STRIDE 1
 3×3 CONV. 512 LEAKYRELU, STRIDE 1
DOWNSCALE
 3×3 CONV. 512 LEAKYRELU, STRIDE 1
 3×3 CONV. 512 LEAKYRELU, STRIDE 1
DOWNSCALE
(OPTIONAL) MINIBATCH DEVIATION LAYER GROUPS OF 4
 3×3 CONV. 256 LEAKYRELU, STRIDE 1
RESHAPE INTO 8192 LENGTH VECTOR
FC TO 512, LEAKYRELU
FC TO 1, *sigmoid*

9.4 Algorithms

Algorithm 1 Overview of RényiGAN- α , RényiGAN- α - L_1 , and RényiGAN-GP- α - L_1 algorithms

Initialize neural networks.

Fix number of epochs n .

for $i = 0$ **to** $n - 1$ **do**

Sample batch size of m noise samples $\{z_1, \dots, z_m\}$ from noise prior p_z

Sample batch size of m examples $\{x_1, \dots, x_m\}$ from the true distribution p_x

Update the discriminator by descending its stochastic gradient without gradient penalty:

$$\nabla_{\theta_D} \left(-\frac{1}{m} \sum_{i=1}^m [\log D(x_i) + \log(1 - D(g(z_i)))] \right)$$

 or with gradient penalty:

$$\nabla_{\theta_D} \left(-\frac{1}{m} \sum_{i=1}^m [\log D(x_i) + \log(1 - D(g(z_i)))] + \gamma \left(\frac{1}{m} \sum_{i=1}^m \left\| \nabla_x \log \left(\frac{D(x)}{1 - D(x)} \right) \Big|_{x=x_i} \right\|_2^2 \right) \right)$$

 and update the generator by descending its stochastic gradient without L_1 normalization:

$$\nabla_{\theta_g} \frac{1}{\alpha - 1} \log \left[\left(\frac{1}{m} \sum_{i=1}^m [1 - D(g(z_i))]^{\alpha-1} \right) \right]$$

 or with L_1 normalization:

$$\nabla_{\theta_g} \left| \frac{1}{\alpha - 1} \log \left[\left(\frac{1}{m} \sum_{i=1}^m [1 - D(g(z_i))]^{\alpha-1} \right) \right] + \log(2) \right|$$

end for

Algorithm 2 Overview of RényiGAN- $[\beta_1, \beta_2]$, RényiGAN- $[\beta_1, \beta_2]$ - L_1 , and RényiGAN-GP- $[\beta_1, \beta_2]$ - L_1 algorithms

Initialize neural networks.

Fix generator's loss function shape, $\alpha_0 = x$, $\text{flag} = \text{True}$ and number of epochs n .

for $i = 0$ **to** $n - 1$ **do**

if flag **then**

$\alpha_i = \alpha_i + 0.1$

if $\alpha_i = \beta_2$ **then**

$\text{flag} = \text{False}$

end if

if $\alpha_i = 1.0$ **then**

$\alpha_i = 1.1$

end if

else

$\alpha_i = \alpha_i - 0.1$

if $\alpha_i = \beta_1$ **then**

$\text{flag} = \text{True}$

end if

if $\alpha_i = 1.0$ **then**

$\alpha_i = 0.9$

end if

end if

Sample batch size of m noise samples $\{z_1, \dots, z_m\}$ from noise prior p_z

Sample batch size of m examples $\{x_1, \dots, x_m\}$ from the true distribution p_x

Update the discriminator by descending its stochastic gradient without gradient penalty:

$$\nabla_{\theta_D} \left(-\frac{1}{m} \sum_{i=1}^m [\log D(x_i) + \log(1 - D(g(z_i)))] \right)$$

or with gradient penalty:

$$\nabla_{\theta_D} \left(-\frac{1}{m} \sum_{i=1}^m [\log D(x_i) + \log(1 - D(g(z_i)))] + \gamma \left(\frac{1}{m} \sum_{i=1}^m \left\| \nabla_x \log \left(\frac{D(x)}{1 - D(x)} \right) \Big|_{x=x_i} \right\|_2^2 \right) \right)$$

without L_1 normalization:

$$\nabla_{\theta_g} \frac{1}{\alpha - 1} \log \left[\left(\frac{1}{m} \sum_{i=1}^m [1 - D(g(z_i))]^{\alpha-1} \right) \right]$$

or with L_1 normalization:

$$\nabla_{\theta_g} \left| \frac{1}{\alpha - 1} \log \left[\left(\frac{1}{m} \sum_{i=1}^m [1 - D(g(z_i))]^{\alpha-1} \right) \right] + \log(2) \right|$$

end for

For the MNIST dataset, the constants for the algorithms are $n = 250$ epochs and batch size

$m = 100$. For both MNIST and CelebA datasets, we chose the gradient penalty scalar $\gamma = 5$.

9.5 Proofs

Proof of Theorem 1 The proof that the solution to (11) is given by $D^* = p_x/(p_x + p_g)$ can be found in the proof of the original GAN result in [15]. Substituting D^* into (13), we have that

$$\begin{aligned}
& \min_g V_\alpha(D^*, g) \\
&= \min_g \left[\frac{1}{\alpha - 1} \log \left(\mathbb{E}_{A \sim p_x} \left[(D^*(A))^{\alpha-1} \right] \right) + \frac{1}{\alpha - 1} \log \left(\mathbb{E}_{B \sim p_z} \left[(1 - D^*(g(B)))^{\alpha-1} \right] \right) \right] \\
&= \min_{p_g} \left[\frac{1}{\alpha - 1} \log \left(\mathbb{E}_{A \sim p_x} \left[(D^*(A))^{\alpha-1} \right] \right) + \frac{1}{\alpha - 1} \log \left(\mathbb{E}_{C \sim p_g} \left[(1 - D^*(C))^{\alpha-1} \right] \right) \right] \\
&\quad (\text{by setting } C = g(B) \text{ and a change of variable}) \\
&= \min_{p_g} \left[\frac{1}{\alpha - 1} \log \left(\mathbb{E}_{A \sim p_x} \left[\left(\frac{2p_x(A)}{p_x(A) + p_g(A)} \right)^{\alpha-1} \right] \right) \right. \\
&\quad \left. + \frac{1}{\alpha - 1} \log \left(\mathbb{E}_{C \sim p_g} \left[\left(\frac{2p_g(C)}{p_x(C) + p_g(C)} \right)^{\alpha-1} \right] \right) \right] - 2 \log(2) \\
&= \min_{p_g} 2 \left[\frac{1}{2} D_\alpha \left(p_x \left\| \frac{p_x + p_g}{2} \right. \right) + \frac{1}{2} D_\alpha \left(p_g \left\| \frac{p_x + p_g}{2} \right. \right) \right] - 2 \log(2) \\
&= \min_{p_g} 2 \text{JR}_\alpha(p_x \| p_g) - 2 \log(2) \\
&= -2 \log(2),
\end{aligned}$$

where the last equality holds since $\text{JR}_\alpha(p_x \| p_g) \geq 0$ and is equal to 0 if and only if $p_g = p_x$ (a.e.). ■

Proof of Theorem 2

The proof of the theorem requires the following result, which we recall from [41].

Lemma 1 For any $x > \frac{1}{2}$,

$$(x - 1) \left(1 + \frac{1 - x}{2} \right) \leq \log(x) \leq x - 1.$$

Recall that $(\mathbb{X}, \mathcal{B}(\mathbb{X}), \mu)$ is the measurable space of images. First, note that by setting

$$x_{1,\alpha} = \mathbb{E}_{A \sim p_x} (D(A))^{\alpha-1}$$

and

$$x_{2,\alpha} = \mathbb{E}_{B \sim p_z} ((1 - D(g(B)))^{\alpha-1}),$$

we have that $\lim_{\alpha \downarrow 1} x_{1,\alpha} = 1$ and $\lim_{\alpha \downarrow 1} x_{2,\alpha} = 1$. Also, Lemma 1 yields that

$$\lim_{\alpha \downarrow 1} \frac{\log(x_{1,\alpha})}{x_{1,\alpha} - 1} = \lim_{\alpha \downarrow 1} \frac{\log(x_{2,\alpha})}{x_{2,\alpha} - 1} = 1.$$

We then can write

$$\lim_{\alpha \downarrow 1} V_\alpha(D, g)$$

$$\begin{aligned}
&= \lim_{\alpha \downarrow 1} \left(\frac{1}{\alpha - 1} \log(x_{1,\alpha}) + \frac{1}{\alpha - 1} \log(x_{2,\alpha}) \right) \\
&= \lim_{\alpha \downarrow 1} \left(\frac{x_{1,\alpha} - 1}{\alpha - 1} \frac{\log(x_{1,\alpha})}{x_{1,\alpha} - 1} + \frac{x_{2,\alpha} - 1}{\alpha - 1} \frac{\log(x_{2,\alpha})}{x_{2,\alpha} - 1} \right) \\
&= \lim_{\alpha \downarrow 1} \left(\frac{x_{1,\alpha} - 1}{\alpha - 1} \right) \lim_{\alpha \downarrow 1} \left(\frac{\log(x_{1,\alpha})}{x_{1,\alpha} - 1} \right) \\
&\quad + \lim_{\alpha \downarrow 1} \left(\frac{x_{2,\alpha} - 1}{\alpha - 1} \right) \lim_{\alpha \downarrow 1} \left(\frac{\log(x_{2,\alpha})}{x_{2,\alpha} - 1} \right) \\
&= \lim_{\alpha \downarrow 1} \frac{x_{1,\alpha} - 1}{\alpha - 1} + \lim_{\alpha \downarrow 1} \frac{x_{2,\alpha} - 1}{\alpha - 1}
\end{aligned}$$

if and only if $\lim_{\alpha \downarrow 1} \frac{x_{1,\alpha} - 1}{\alpha - 1}$ and $\lim_{\alpha \downarrow 1} \frac{x_{2,\alpha} - 1}{\alpha - 1}$ both exist. We next show the existence of these limits and verify that their sum is indeed equal to $V(D, g)$. Consider

$$\lim_{\alpha \downarrow 1} \frac{x_{1,\alpha} - 1}{\alpha - 1} = \lim_{\alpha \downarrow 1} \int_{\mathbb{X}} \frac{p_x \times D^{\alpha-1} - p_x}{\alpha - 1} d\mu.$$

In order to invoke the monotone convergence theorem, we prove that the integrand is non-increasing and bounded above as $\alpha \downarrow 1$. Noting that

$$\begin{aligned}
&\frac{d}{d\alpha} \frac{p_x \times D^{\alpha-1} - p_x}{\alpha - 1} \\
&= \frac{p_x + [(\alpha - 1) \log(D) - 1] \times p_x \times D^{\alpha-1}}{(\alpha - 1)^2},
\end{aligned}$$

it is enough to show that

$$p_x + [(\alpha - 1) \log(D) - 1] \times p_x \times D^{\alpha-1} \geq 0.$$

Indeed, we have

$$\begin{aligned}
p_x [1 + [\log(D^{\alpha-1}) - 1] \times D^{\alpha-1}] &\geq p_x \left[1 + \left[1 - \frac{1}{D^{\alpha-1}} - 1 \right] \times D^{\alpha-1} \right] \\
&= p_x [1 - 1] \\
&= 0,
\end{aligned} \tag{17}$$

where (17) holds since $\log(x) \geq 1 - \frac{1}{x}$, for $x > 0$. We next show that the integrand is bounded from above. The upper bound can be obtained by letting $\alpha \rightarrow \infty$:

$$\lim_{\alpha \rightarrow \infty} \frac{p_x \times D^{\alpha-1} - p_x}{\alpha - 1} = 0.$$

Hence, by the monotone convergence theorem, we have that

$$\lim_{\alpha \downarrow 1} \int_{\mathbb{X}} \frac{p_x \times D^{\alpha-1} - p_x}{\alpha - 1} d\mu = \int_{\mathbb{X}} \lim_{\alpha \downarrow 1} \frac{p_x \times D^{\alpha-1} - p_x}{\alpha - 1} d\mu.$$

Finally by L'Hôpital's rule, we obtain that

$$\lim_{\alpha \downarrow 1} \frac{x_{1,\alpha} - 1}{\alpha - 1} = \int_{\mathbb{X}} \frac{p_x \log(D)}{1} d\mu = \mathbb{E}_{A \sim p_x} [\log(D(A))].$$

The proof of

$$\begin{aligned}\lim_{\alpha \downarrow 1} \frac{x_{2,\alpha} - 1}{\alpha - 1} &= \int_{\mathbb{X}} \frac{p_z \log(1 - D(g))}{1} d\mu \\ &= \mathbb{E}_{B \sim p_z} [\log(1 - D(g(B)))]\end{aligned}$$

is similar. We thus conclude that

$$\lim_{\alpha \downarrow 1} V_\alpha(D, g) = V(D, g).$$

Next, we shall prove (15) by taking $\alpha \uparrow 1$. For $\alpha < 1$, $x_{1,\alpha} = \mathbb{E}_{A \sim p_x} (D(A)^{\alpha-1}) < \infty$ and $x_{2,\alpha} = \mathbb{E}_{A \sim p_z} ((1 - D(g(A)))^{\alpha-1}) < \infty$, by the fact that $x_{1,\alpha}$ and $x_{2,\alpha}$ are non-increasing in $\alpha > 0$ and by the assumption that $\mathbb{E}_{A \sim p_x} \left(\frac{1}{D(A)} \right) < \infty$ and $\mathbb{E}_{A \sim p_z} \left(\frac{1}{1 - D(g(A))} \right) < \infty$. Hence, $\lim_{\alpha \uparrow 1} x_{1,\alpha} = \lim_{\alpha \uparrow 1} x_{2,\alpha} = 1$. Using Lemma 1, we can apply the same steps as above with the alteration of the following argument. Consider

$$\lim_{\alpha \uparrow 1} \frac{x_{1,\alpha} - 1}{\alpha - 1} = \lim_{\alpha \uparrow 1} \int_{\mathbb{X}} \frac{p_x \times D^{\alpha-1} - p_x}{\alpha - 1} d\mu.$$

We know that the integrand is non-decreasing in α . To use the monotone convergence theorem, we need to show that the integrand is bounded below. Note that

$$\lim_{\alpha \rightarrow 0} \frac{p_x \times D^{\alpha-1} - p_x}{\alpha - 1} = p_x - \frac{p_x}{D}.$$

Since we assumed $\mathbb{E}_{A \sim p_x} \left(\frac{1}{D(A)} \right) < \infty$, we have that $\frac{p_x}{D} < \infty$ almost everywhere. As a result, the integrand is bounded below (a.e.). Following the same steps as in the previous part, we conclude that

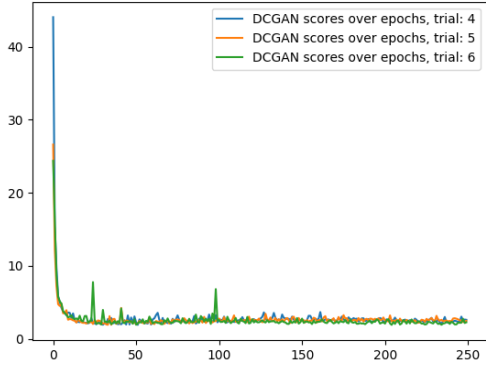
$$\lim_{\alpha \uparrow 1} V_\alpha(D, g) = V(D, g).$$

■

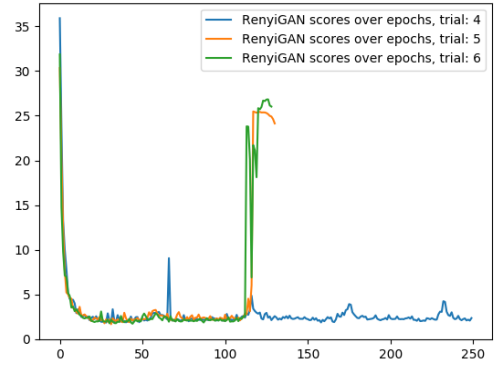
9.6 MNIST: full FID scores, FID vs epoch plots and sample generated images

Table 8: The best FID scores taken over 250 epochs for each trial.

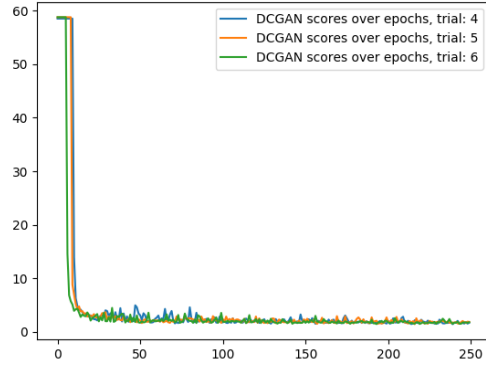
Trial number	1	2	3	4	5	6	7	8	9	10
RényiGAN-0.5- L_1	2.20	2.32	2.18	2.36	2.13	2.15	2.31	2.10	2.13	2.17
RényiGAN-3.0- L_1	1.84	1.83	1.81	1.81	1.87	1.69	1.83	1.72	1.81	1.76
RényiGAN-[0, 0.9]- L_1	1.99	2.24	2.22	2.07	2.14	2.16	2.25	2.10	2.21	2.19
RényiGAN-[0, 3]- L_1	1.88	1.81	1.75	1.74	1.66	1.71	1.85	1.73	1.84	1.70
RényiGAN-[1.1, 4]- L_1	1.76	1.77	1.75	1.84	1.86	1.92	1.83	1.80	1.73	1.80
DCGAN- L_1	2.02	1.89	1.92	1.91	1.91	1.90	2.02	1.88	1.85	2.03
RényiGAN-GP-0.5	1.48	1.41	1.45	1.35	1.32	1.37	1.26	1.37	1.38	1.28
RényiGAN-GP-3.0	1.34	1.43	1.32	1.25	1.39	1.39	1.42	1.38	1.36	1.36
RényiGAN-GP-[0, 0.9]	1.46	1.28	1.37	1.37	1.37	1.40	1.41	1.34	1.35	1.28
RényiGAN-GP-[0, 3]	1.43	1.42	1.52	1.37	1.46	1.34	1.36	1.36	1.45	1.36
RényiGAN-GP-[1.1, 4]	1.33	1.39	1.54	1.37	1.35	1.36	1.29	1.36	1.33	1.32
DCGAN-GP	1.38	1.29	1.34	1.39	1.39	1.41	1.37	1.32	1.32	1.34
RényiGAN-GP-0.5- L_1	1.14	1.24	1.16	1.16	1.18	1.18	1.08	1.27	1.14	1.23
RényiGAN-GP-3.0- L_1	1.21	1.14	1.17	1.14	1.14	1.20	1.06	1.30	1.13	1.20
RényiGAN-GP-[0, 0.9]- L_1	1.26	1.15	1.28	1.16	1.10	1.17	1.10	1.21	1.21	1.24
RényiGAN-GP-[0, 3]- L_1	1.29	1.28	1.32	1.19	1.14	1.14	1.12	1.19	1.35	1.18
RényiGAN-GP-[1.1, 4]- L_1	1.29	1.14	1.31	1.19	1.19	1.14	1.20	1.18	1.25	1.14
DCGAN-GP- L_1	1.21	1.26	1.20	1.15	1.15	1.19	1.13	1.19	1.13	1.16



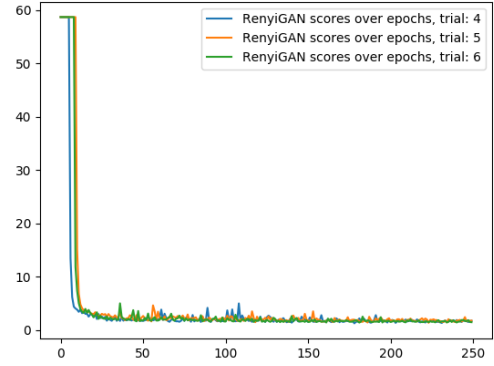
(a) FID scores vs epochs for DCGAN- L_1 .



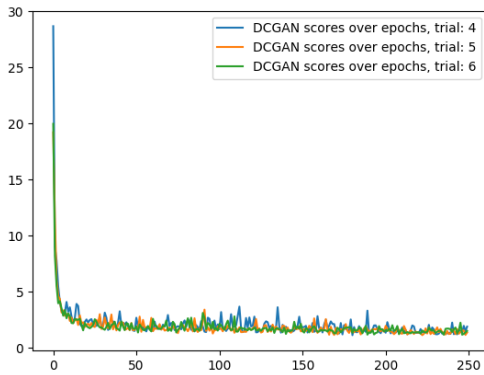
(b) FID scores vs epochs for RényiGAN-[0, 3]- L_1 .



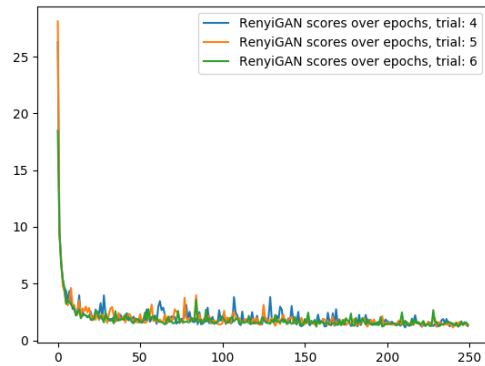
(c) FID scores vs epochs for FID score.



(d) FID scores vs epochs for RényiGAN-GP-3.0.

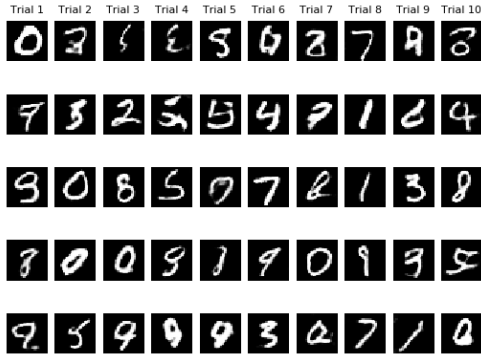


(e) FID scores vs epochs for DCGAN-GP- L_1 .

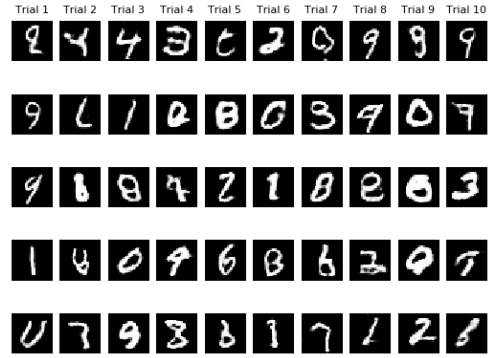


(f) FID scores vs epochs for RényiGAN-GP-3.0- L_1 .

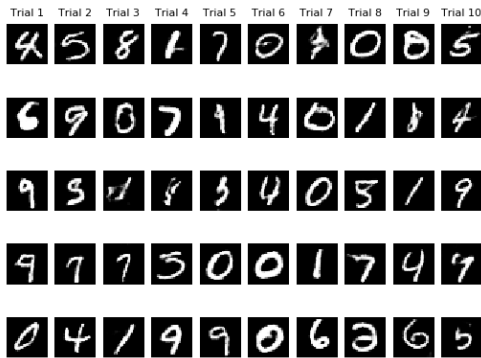
Figure 2: MNIST: plots of FID scores versus epochs.



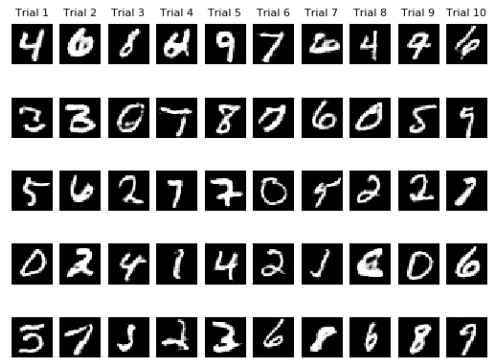
(a) Sample images of DCGAN- L_1 with average best FID score of 1.93



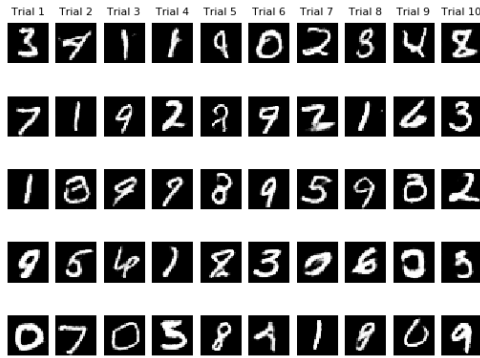
(b) Sample images of RényiGAN-[0,3]- L_1 with average best FID score of 1.77



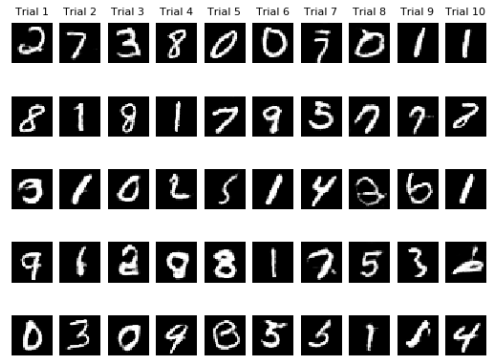
(c) Sample images of DCGAN-GP with average best FID score of 1.36



(d) Sample images of RényiGAN-GP-3.0 with average best FID score of 1.36



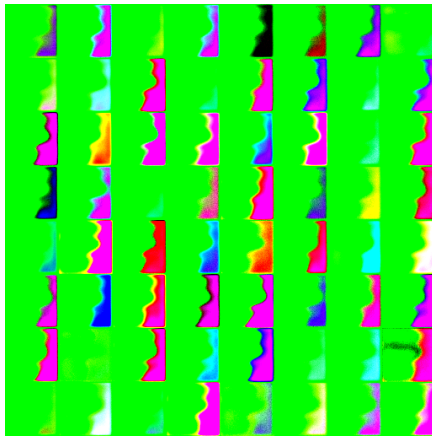
(e) Sample images of DCGAN-GP- L_1 with average best FID score of 1.18



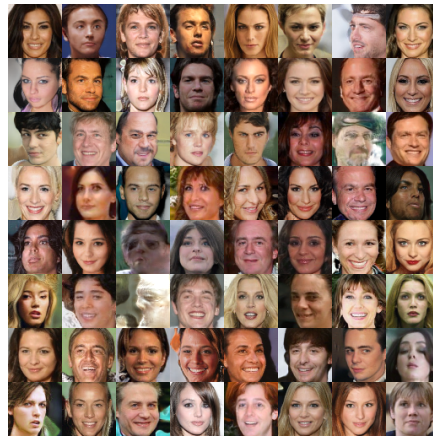
(f) Sample images of RényiGAN-GP-3.0- L_1 with average best FID score of 1.17.

Figure 3: Sample generated images of best performing RényiGAN in terms of FID scores for each group and their DCGAN counterparts.

9.7 CelebA: sample generated images



(a) RényiStyleGAN0.5



(b) RényiStyleGAN3.0



(c) RényiStyleGAN9.0



(d) StyleGAN



(e) RényiStyleGAN3.0-GP



(f) StyleGAN-GP

Figure 4: Uncurated samples taken from various StyleGAN architectures. For each variant, the best model over the trials was selected for visualization.